Breakdown of scaling in droplet fission at high Reynolds number

Michael P. Brenner
Department of Mathematics, Massachusetts Institute of Technology, Cambridge, Massachusetts 02139

Jens Eggers
Universität Gesamthochschule Essen, Fachbereich Physik, 45117 Essen, Germany

Kathy Joseph, Sidney R. Nagel, and X. D. Shi
James Franck Institute, University of Chicago, Chicago, Illinois 60637

(Received 8 July 1996; accepted 30 January 1997)

In this paper we address the shape of a low-viscosity fluid interface near the breaking point. Experiments show that the shape varies dramatically as a function of fluid viscosity. At low viscosities, the interface develops a region with an extremely sharp slope, with the steepness of the slope diverging with vanishing viscosity. Numerical simulations demonstrate that this tip forms as a result of a convective instability in the fluid; in the absence of viscosity this instability results in a finite time singularity of the interface far before rupture (in which the interfacial curvature diverges). The dynamics before the instability roughly follow the scaling laws consistent with predictions based on dimensional analysis, though these scaling laws are violated at the instability. Since the dynamics after rupture is completely determined by the shape at the breaking point, the time dependences of recoiling do not follow a simple scaling law. In the process of demonstrating these results, we present detailed comparisons between numerical simulations and experimental drop shapes with excellent agreement. © *1997 American Institute of Physics.*
[S1070-6631(97)00306-1]

I. INTRODUCTION

Droplet breakup has been a subject of scientific scrutiny for over 100 years. Early contributions include Plateau's description of the instability mechanism,[1] Lord Rayleigh's calculation of the most unstable wavelength,[2] Worthington's pictures of splashes,[3] and Edgerton's high-speed stroboscopic photographs,[4–6] which first revealed the intricate shapes during rupture.

In the 1970's, there was a resurgence of interest in jet breakup,[7–11] mainly driven by its technological relevance (e.g., to ink jet printing). Detailed experiments studied the dynamics of both high- and low-viscosity fluid jets emanating from a nozzle, focusing on the early stages of pinching. A principal goal of this work was to understand the control of the size distribution of satellite droplets. More recently, numerical methods have been developed to study jet decay, based on the assumption of inviscid, irrotational flow[12] or highly viscous Stokes flow.[13–15]

From a mathematical point of view droplet breakup provides a simple example of singularity formation.[16–19] Starting from a smooth initial shape with finite fluid velocities, a breaking drop develops singularities in a finite amount of time in which physical quantities, such as the curvature of the interface or the fluid velocity, diverge. A fundamental question is to determine the nature of the flow in the neighborhood of the singularity.

For a liquid drop breaking in vacuum, the shape near the breaking point depends critically on the viscous length scale, first identified by Peregrine *et al.*,[20] defined as

$$l_\nu = \frac{\nu^2 \rho}{\gamma},$$

where ν is the kinematic viscosity, γ the surface tension, and ρ the fluid density. Figure 1 shows several shapes for three different fluid viscosities: the radius of the water neck [Fig. 1(a)] is much larger than the viscous length scale, which is only 140 Å. Increasing the viscosity by a factor of 100 [Fig. 1(b)] leads to a 10^4 increase in l_ν. At such a high viscosity, the shape is slender near the breaking point. For even higher-viscosity fluids like glycerol ($l_\nu = 1$ cm) the slenderness is more pronounced [Fig. 1(c)], with a much more gradual teardrop shape.

The goal of the present paper is to understand the qualitative differences between the shapes in these pictures: at high viscosities, the connection of the fluid thread to the drop is gradual [Fig. 1(c)], whereas at low viscosities the shape is highly asymmetric, with an abrupt transition from the thread to the drop separated by a region of extremely steep slope [Fig. 1(a)]. In fact, as will be shown below through experiments and numerical simulations, the steepness of the slope actually diverges with vanishing viscosity. Through a combination of numerical simulations and experiments, we will attempt to answer the following questions: What sets the scale of the asymmetry? How does the asymmetry vary with fluid viscosity? And how does this asymmetry arise from the dynamics leading to droplet fission?

In addressing these questions, our study will focus on a fundamental idea about how liquid drops break, originally introduced by Keller and Miksis:[21] Arbitrarily close to the breaking point there are no external length scales describing the interface, so the dynamics should be *self-similar*:[22] the shape of the interface when the minimum radius is 1 μm should be the same as the shape when the minimum radius is 10 μm, modulo rescalings of the axes. Peregrine *et al.* refined this idea[20] and applied it to their experiments on falling water drops: They point out that for low-viscosity fluids

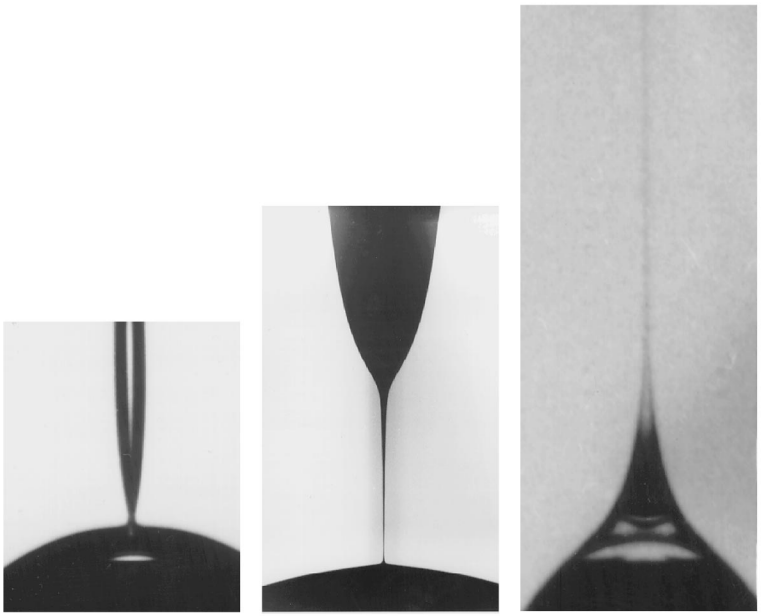

FIG. 1. Shape of the fluid interface immediately before rupture, for three different viscosities. (a) is water $\nu_{H_2O}=0.01$ cm^2/s; (b) is a 85 wt. % glycerol water mixture with a viscosity $\nu=100\nu_{H_2O}$; (c) is pure glycerol with viscosity $\nu=1200\nu_{H_2O}$.

there is a range of scales where the thickness of the fluid neck is much larger than the viscous length scale l_ν, but much smaller than the length scale, where energy is fed into the system. Over this range of scales, the self-similarity hypothesis might be expected to hold. For high-viscosity fluids, the thickness of the thread is usually much smaller than l_ν, so that self-similarity will also hold.

These considerations suggest that a breaking fluid interface should be described by a similarity solution to the governing hydrodynamic equations. The first study to our knowledge that succeeded in constructing a similarity solution for a breaking fluid thread was for the rupture of a drop in the two-dimensional Hele–Shaw cell.[16,17] This initial success was followed up with the identification of further similarity solutions for the Hele–Shaw cell,[19,23] as well as the discovery of a similarity solution for three-dimensional droplet fission for fluid threads with thickness much smaller than l_ν.[24–26] In this case the similarity solution is unstable to finite-amplitude perturbations,[27] with the critical amplitude for instability approaching zero at the singularity.[28] At the high viscosities where this similarity solution is relevant, the droplet shape is long and slender, as apparent in Fig. 1(c).

The question addressed in this paper is whether similar scaling ideas can explain the interfacial shapes during the breakup of low-viscosity fluids, such as the water drop in Fig. 1(a). Based on the above discussion, this translates into the question of whether the self-similar singularities in the equations of *inviscid* hydrodynamics describe experiments when the thread thickness is larger than the viscous length scale l_ν? To answer this question, we will describe in detail the characteristics of a water drop falling from a nozzle both before and after a fission event. Through a combination of experiments, numerical simulations, and theory, we argue that the scaling hypothesis fails for this problem. When the thread thickness is far greater than the viscous length (10^5 times greater for a water drop falling from a 4 mm nozzle), a dynamical instability produces another small length scale, which destabilizes the similarity solution. In the absence of viscosity, this instability actually causes a singularity in the curvature of the interface before rupture occurs. This instability of the scaling solution at low viscosities provides a natural explanation for the steep front in water drops [Fig. 1(a)]. Although there is no inviscid singularity after breakup, the scaling behavior before breakup is imprinted on the time dependences after breakup,[29] since the solution at the time of breakoff provides an initial condition for the recoiling; the shape at the rupture point is not a perfect power law, which results in a more complicated time dependence than power law scaling.

The paper is organized as follows: The second section introduces the experimental and theoretical frameworks by presenting a detailed comparison between a numerical simulation of a drop falling from a faucet and experimental photographs. The simulations use a one-dimensional ''long-wavelength'' approximation to the full hydrodynamic equations developed previously.[24,30,31] The agreement between simulations and experiment is remarkably good, with simulations reproducing detailed features of the experiment, even though the long-wavelength assumption does not hold uniformly throughout the breaking. The next two sections study in detail the solution near the breaking point in the low-viscosity limit. In Sec. III we address solutions before breakup, while in Sec. IV we address the situation after breakup. In both cases we combine available theoretical, experimental, and simulational evidence to provide a complete picture of the singularities.

II. FORMULATION OF PROBLEM

The experimental configuration addressed in this paper is the falling of a drop from a circular nozzle. We consider the limit of slow dripping: the drop is adiabatically filled with fluid until the shape becomes unstable. Two dimensionless parameters characterize this situation: the Bond number,

$$\mathrm{Bo}=R^2\rho g/\gamma;$$

and the Reynolds number,

$$\mathrm{Re}=(R/l_\nu)^{1/2}.$$

Here R is the radius of the nozzle, g is the gravitational acceleration, and ρ, l_ν, and γ are the fluid parameters defined above.

Several groups have recently studied large-scale features of a drop dripping from a circular nozzle.[20,27,32] Here, we are primarily concerned with the nature of singularities in the limit of zero viscosity (infinite Reynolds number). Near the rupture, there is a large separation between the time scale of the flow at the singularity and the time scales characterizing flow fields far from the breaking point. Thus, it is expected that properties of singularity formation are only weakly dependent on the specific experimental setup—in this case the Bond number Bo. The results of this paper should therefore apply to droplet breakup at high Reynolds number in any experimental configuration. Indeed, Edgerton's initial observation of sharp interfaces in low viscosity fluids occurred in several experimental setups, ranging from his famous pictures of splashes[4] to fluid falling from a nozzle.

The goal of this section is twofold: first we describe a simplified model for understanding the drop dynamics. An inviscid version of this model was first proposed by Lee,[33] viscosity was later included by Bechtel, Forest, and Lin,[30] Eggers and Dupont,[24] and Sellens.[31] Then, we present two sets of experiments and simulations and compare the results. The first set studies a water drop falling from a nozzle, while the second set focuses separately on the thin neck region separating the drop from the nozzle. Eggers and Dupont[24] already presented such a comparison for Peregrine's photograph of a water drop immediately before it breaks. Here we continue the simulations through the rupture of the initial drop and the satellite drops until the original drop is separated from the nozzle by several smaller satellite drops. The simulations continue to describe the experiment, even for the nearly spherical satellite drops, when the long wavelength approximation clearly no longer holds.

The experiments consisted of photographing a low-viscosity fluid, deionized water at room temperature, dripping from a thin vertical nozzle. The rate of drop formation at the nozzle was kept small so that the initial velocities could be assumed to be negligible. This was determined by decreasing the rate of flow until the macroscopic shape of the drop no longer varied with the rate. The diameter of the nozzle could be varied. The photographs were taken in two ways. In order to determine the shape of the drop as a function of time, we used a HyCam 400 16 mm movie camera, which, with its quarter-frame attachment, could take a maximum of 44 000 frames per second. In order to measure the movement of the drop as a function of time, the frames from the HyCam were transferred onto videotape and analyzed with a computer. For precision pictures of the droplet shape, we used a medium format camera with an open shutter and a strobe. When the drop began to fall, it interrupted a laser beam incident upon a photodiode. After a variable time delay, this triggered a fast 5 MS EG and G MVS-2601 Strobe. In both cases, the lighting was from the rear so that the liquid/air interface would be plainly visible. (Since the drop acts like a small lens, the edges of the liquid appear black and bright spots appear along the axis.) For close-up photography, the lens was attached via a bellows to the camera.

The mathematical problem assumes the dynamics of an axisymmetric column of fluid with kinematic viscosity ν, density ρ, and surface tension γ falling in vacuum. The fluid moves via the incompressible Navier–Stokes equations, augmented with the two boundary conditions that (i) normal stresses are proportional to the mean curvature and (ii) tangential stresses are zero. The final condition is that the interface moves with the fluid.

The full hydrodynamic equations are difficult to understand theoretically or simulate numerically. We instead consider a long-wavelength approximation of the full equations[24,30,31] by systematically expanding the full equations in powers of a slenderness parameter. Another derivation of the long-wavelength equations, is presented in Appendix A, which elucidates the physical constraints: The form of the equations is fixed by seeking the simplest nonlinear equations that preserve the conservation laws (mass and momentum) of the flow, while preserving Galilean invariance, an idea that is quite old.[34,35] The only nontrivial term describes viscous dissipation: this term follows by demanding that the equations also generate the same dispersion relation of long-wavelength disturbances as the full hydrodynamic equations. The evolution equations for the interface radius $h(z,t)$ and the velocity field $v(z,t)$ are

$$(h^2)_t=-(h^2v)_z, \tag{1}$$

$$v_t+vv_z=\frac{3}{\mathrm{Re}\ h^2}(h^2v_z)_z-\kappa_z+\mathrm{Bo}, \tag{2}$$

$$\kappa=\left(\frac{1}{h\sqrt{1+h_z^2}}-\frac{h_{zz}}{(\sqrt{1+h_z^2})^3}\right), \tag{3}$$

where we have nondimensionalized all lengths by the nozzle radius R, and all times by the basic time scale

$$\tau=\sqrt{\frac{\rho R^3}{\gamma}}. \tag{4}$$

Note that the equations as written above violate the asymptotic derivation in powers of the slenderness parameter,[36] since they selectively include higher-order terms in h_z. Specifically, it would be asymptotically correct to approximate $\sqrt{1+h_z^2}\approx 1$, and also to neglect the h_{zz} term entirely.[36] The reason for including these terms is twofold: first, only by keeping the higher-order terms in the pressure do the equations have the correct equilibrium shapes, which is important for capturing the flow away from the breaking point.[24] Second, even starting from a cylinder as an initial condition, the asymptotic equations show exponential growth

at arbitrarily short wavelengths. In simulations, this shows up as rapidly growing oscillations on the scale of the computational grid, which would have to be damped out by some *ad hoc* method without the presence of the higher-order terms.

The numerical simulations solve a finite difference version of the lubrication approximation discussed above. The details of the finite difference method have previously been discussed in several places.[16,24,19,27] We briefly summarize the major points of the simulations; technical details are reserved for Appendix B. The finite difference equations are solved implicitly, resulting in a system of nonlinear equations at each time step, which are solved using Newton's method. The time step is dynamically adjusted to control several different indicators of the numerical error. The code employs a dynamically evolving mesh, which is essential for obtaining the level of resolution necessary to resolve the breaking adequately. The mesh is adjusted whenever prespecified conditions on the solution are satisfied. When the minimum thickness of the droplet drops below a threshold, the code ''breaks'' the drop, by dividing the computational domain into two pieces and then interpolating the shape of the interface around the breaking point. Once the drop is artificially broken, the equations are solved at each mesh point. Numerical tests demonstrate that the large-scale results are independent of the method of cutting the thread; in particular, decreasing the threshold thickness for ''breaking'' does not affect any of the results. The details associated with implementing this procedure efficiently are discussed in Appendix C. A typical simulation lasts a few hours on a SUN Sparc 20.

As an illustration of how closely simulations match the experiment, in the following figures we focus on a water drop falling from a $R=1.5$ mm nozzle ($\mathrm{Bo}=0.3$, $\mathrm{Re}=330$). In both experiments and simulations, the drop is slowly filled with fluid, passing through a sequence of equilibrium shapes; at a critical volume, the drop falls from the nozzle. Figure 2 shows both experimental photographs and simulations at different stages of the breaking: Initially the drop hangs from the nozzle in equilibrium. Then the drop falls, pulling out a thin neck that separates it from the nozzle [Fig. 2(a)]. After breaking [which occurs between the times of Fig. 2(b) and Fig. 2(c)], the drop continues to fall, while the thin neck recoils toward the nozzle [Fig. 2(c)]. As the thin neck recoils, capillary waves are generated and propagate towards the nozzle. These waves are excited since the wave speed for capillary waves coincides with the retraction speed of the fluid neck (see Appendix C). Then the recoiling neck breaks at the top of the thin neck, near the nozzle [Fig. 2(d)].

It should be emphasized that the simulation contains no free parameters: given the dimensionless Bond number Bo and Reynolds number Re the shapes are uniquely determined by the dynamics. We find it remarkable that such a simple model can capture so many details of the breaking process.

It should be noted, however, that these simulations cannot capture all qualitative aspects of the experiments: in particular, simulations of the long-wavelength equations are not capable of *overturning*, where the thickness $h(z)$ becomes double valued. Close examination of movies of water drops shows that overturning never occurs before the initial fission event, but does tend to occur during the oscillations of the satellite drops. Typically, overturning in satellite drop oscillations occurs for experiments with larger nozzles (Bond numbers) than Fig. 2. The long-wavelength equations avoids overturning (which would result in a singularity) by producing a large amount of dissipation where overturning is about to occur. This feature allows the simulations to be continued to arbitrarily long times; however, the agreement between simulations and experiments degrades after an (experimental) overturning event.

Recently, Schulkes[37] performed a boundary integral simulation of an *inviscid, irrotational* fluid dripping from a nozzle, and presented a detailed comparison of his simulations with the Peregrine *et al.*[20] experiments on water drops. An interesting difference between the present simulations and Schulkes' inviscid simulations is that the latter demonstrate overturning *before* the initial fission event, whereas the former do not. The reason for this difference will be elaborated in detail below: Based on comparisons of experiments and simulations, we argue that this difference is because the long-wavelength equations more accurately describe the dynamics than the assumption that the flow is inviscid and irrotational. Our simulations show that viscosity is a singular perturbation to the dynamics in the long-wavelength equations; the inclusion of an (arbitrarily small) amount of viscosity stops overturning during rupture. The agreement between these simulations and experiments leads us to conjecture that the full equations also contain this singular viscosity dependence.

Now we summarize another set of simulations and experiments to be used in the remainder of the paper in analyzing the dynamics of the rupture. Immediately after rupture, the interface (when viewed on a length scale larger than the viscous scale) consists of a sharp conical tip attached to a spherical shell. Figure 3 shows a sequence of the recoil from both simulations and experiments, for a water drop falling from a $R=3.5$ mm pipette ($\mathrm{Bo}=6.5$, $\mathrm{Re}=500$). The initial state of the drop was prepared exactly in the manner as for the previous simulation (i.e., by passing through a sequence of equilibrium shapes). We show only the thin neck region separating the drop of fluid from the nozzle, since this is the relevant regime for the analysis in the following sections; however, we emphasize that the agreement between simulations and experiments persists throughout the entire drop, as demonstrated in the previous figure. The speed of the photography was enhanced by a factor of 4 by printing four successive pictures (separated in time by 2.5×10^{-5} s) on a single frame of film. In each frame, the earliest time is printed at the bottom, and latest frame at the top. The fourfold increase in the timing gained allows a more precise analysis of the singularity reported in Sec. IV.

III. SHAPES NEAR RUPTURE

In the remainder of this paper, we analyze the pictures aiming at a complete description of the interfacial shapes and fluid velocities close to a breaking event. For water drops, the viscous length scale $l_\nu\approx0.01$ μm is much smaller than the length scales visible in the photographs (larger than 1

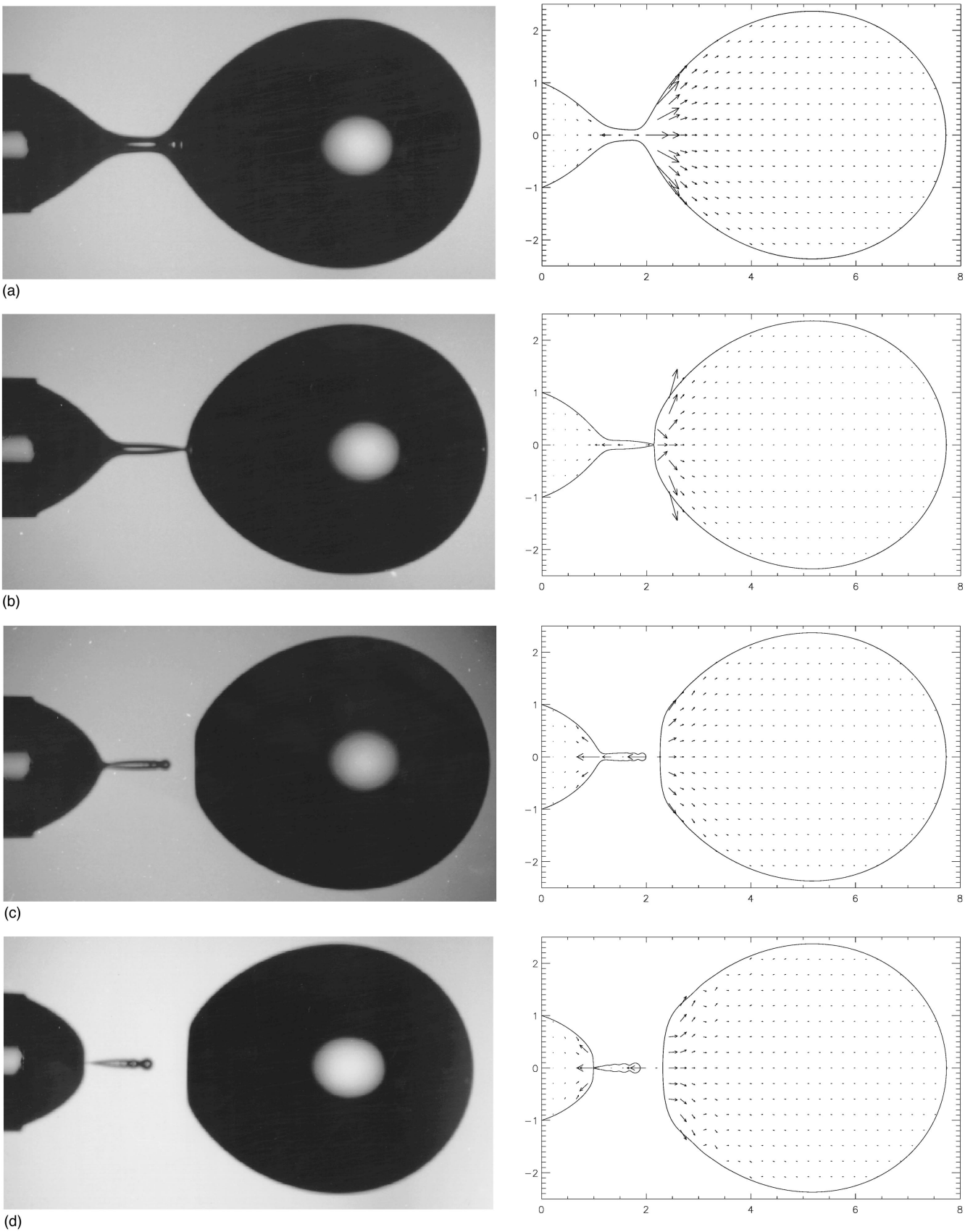

FIG. 2. Left panel: Photographs of a water drop falling from a nozzle with radius $R=1.5$ mm (Bo$=0.3$, Re$=330$). The nozzle is visible at the top of the picture. Right panel: Sequence of shapes from numerical simulations of Eqs. (1)–(3) for the same configuration. The times were chosen so that the drop shapes match the experiments. Length scales are in units of the droplet radius. In both simulations and experiments a pendant drop is filled adiabatically until it becomes unstable and falls.

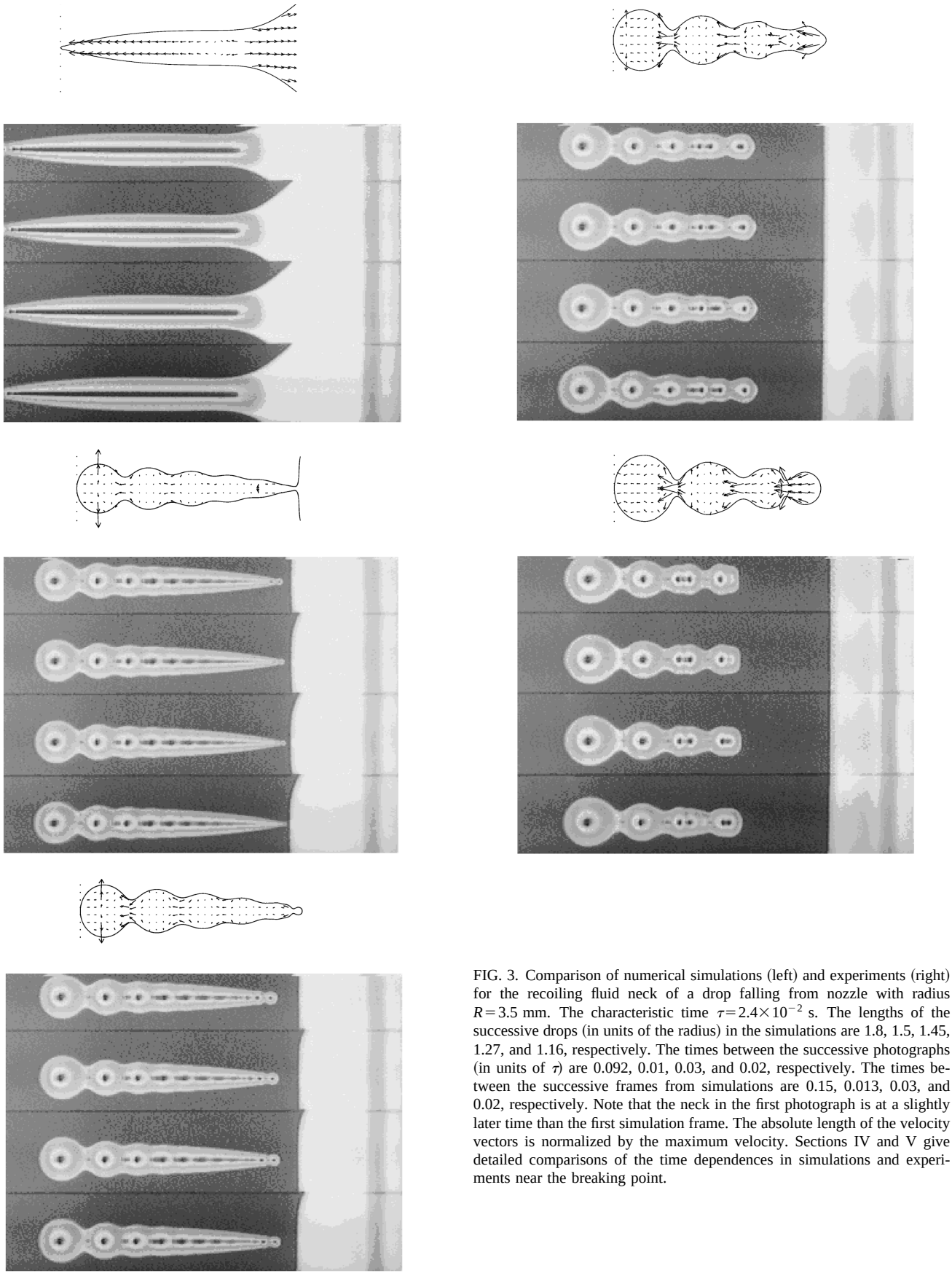

FIG. 3. Comparison of numerical simulations (left) and experiments (right) for the recoiling fluid neck of a drop falling from nozzle with radius $R=3.5$ mm. The characteristic time $\tau=2.4\times10^{-2}$ s. The lengths of the successive drops (in units of the radius) in the simulations are 1.8, 1.5, 1.45, 1.27, and 1.16, respectively. The times between the successive photographs (in units of τ) are 0.092, 0.01, 0.03, and 0.02, respectively. The times between the successive frames from simulations are 0.15, 0.013, 0.03, and 0.02, respectively. Note that the neck in the first photograph is at a slightly later time than the first simulation frame. The absolute length of the velocity vectors is normalized by the maximum velocity. Sections IV and V give detailed comparisons of the time dependences in simulations and experiments near the breaking point.

μm). This separation of scales leads to the expectation that the viscous stresses should *always* be much smaller than the other forces when the drop thickness is much larger than l_ν. If this is true, then the viscous term $3(\mathrm{Re}\, h^2)^{-1}(v_z h^2)_z$ in Eq. (2) can simply be dropped when analyzing the flow field: thus, *inviscid* hydrodynamics might be expected to be sufficient for describing rupture.

In their classical paper,[21] Keller and Miksis advanced a dimensional argument suggesting the time dependences of a recoiling inviscid wedge. Their argument is sufficiently general that it applies to the inviscid dynamics of any surface tension driven flow near a singularity.[38] The application to droplet breakup was emphasized by Peregrine.[20] When viscosity is unimportant, the only relevant dimensional parameters near the singularity are surface tension γ and the fluid density ρ, since the external forcing and initial conditions are assumed to be unimportant. Using these parameters and the dimensional time interval Δt from the singularity (either before or after), only one length scale can be formed, namely

$$\left(\frac{\gamma}{\rho}\right)^{1/3}(\Delta t)^{2/3}. \tag{5}$$

In dimensionless units, with $t'=\Delta t/\tau$ the dimensionless time interval to the singularity, this length is $l(t')=t'^{1/3}$. If l is indeed the only length scale governing the dynamics, then the shape and velocity field should obey a similarity solution of the form

$$h(z,t)=l(t')H\left(\frac{z'}{l(t')}\right), \tag{6}$$

$$v(z,t)=\frac{l(t')}{t'}\,V\left(\frac{z'}{l(t')}\right), \tag{7}$$

where $z'=z-z_0$ is the position relative to the point of breakup z_0. These equations are exact solutions of the equations (1)–(3) at zero viscosity.

The question is whether this dimensional argument suffices to explain the experiments and simulations presented above. There are two assumptions hidden within the argument, which could cause it to fail in practice: First, it is assumed that when the interfacial thickness is larger than the viscous length scale the viscous stresses are irrelevant; there might be dynamical mechanisms that make viscosity important on a length scale different from the viscous length scale l_ν. Second, it is assumed that the singular solution is not at all affected by the outer length scales, i.e., those set by boundary conditions at the nozzle or initial conditions. Although it is generally true that scaling exponents are independent of outer scales, it is often the case that prefactors do depend on outer length scales. The mechanism for this is that the singular solution must be *matched* to the solution far from the singularity, which generically introduces constants in the singular region depending on the outer scales.

We will demonstrate below that *before* breakup the dimensional scaling law fails because viscosity becomes important when the drop radius is much larger than the viscous scale. This fact was already indicated by Eggers and Dupont,[24] and is a consequence of an intrinsic instability in the inviscid equations: without viscosity, the momentum equation resembles a forced kinematic wave equation, in which high-velocity regions move faster than low-velocity regions. This leads to an instability that forms discontinuities in velocity gradients in finite time. The continuity equation implies that a discontinuity in a velocity gradient also causes a discontinuity in the slope of the drop. A finite but arbitrarily small viscosity changes the situation drastically: the steepening of the gradients is stopped by viscous stresses before the interfacial curvature diverges. The viscosity sets the value of the maximum curvature, and thus the maximum slope, and therefore has macroscopic consequences on scales of the order of the drop radius, *even* when l_ν is infinitesimal. This instability provides a natural explanation for the striking difference between the interfacial shapes near rupture for fluids of different viscosity (see Fig. 1). At low viscosity this additional singularity causes the sharp front observed in experiments.

The initial recoiling after breakup for fluid dripping from a nozzle does not manifest the inviscid convective instability just described: We show in Appendix C that when starting from a cone as the initial condition, simulations obey the dimensional scaling laws discussed above. However, because of the breakdown of scaling before breakup, the shape at the rupture point deviates from a cone on scales much larger than l_ν. Using mass and momentum conservation, Keller[29] showed that the initial conditions directly affect the dynamics after breakup. Therefore, after breakup a simple scaling will only be observed over a range of scales set by how closely the shape at the rupture point is a pure power law.

A particularly sharp way of illustrating this problem is the set of scaling solutions for the recoiling of an inviscid drop proposed by Ting and Keller.[39] They pointed out that there are actually a continuous family of other possible similarity solutions to the lubrication equations other than (6) and (7).[39] The more general form,

$$h(z,t)=l_{\mathrm{radial}}(t')H\left(\frac{z'}{l_{\mathrm{axial}}(t')}\right), \tag{8}$$

is also a possible solution to the dynamical equations as $t'\to 0$ as long as

$$l_{\mathrm{radial}}=R(l_{\mathrm{axial}}/R)^{\beta}. \tag{9}$$

These solutions are consistent with the long-wavelength assumption whenever $\beta>1$, so that l_{radial} goes to zero faster than l_{axial}. Note that these solutions require the introduction of an additional length scale R. Correspondingly, the solutions (8) and (9) also have a different asymptotics *away* from the singularity: since the solution must be time independent far from the breaking point, the scaling function $H(\xi)$ must obey $H(\xi)\sim\xi^{\beta}$ at large ξ, so that $h(z)\sim z^{\beta}$.

IV. SHAPES BEFORE BREAKUP

In this section we analyze the dynamics before rupture to establish the claims made above. We begin by measuring the characteristic thickness $h_{\min}$ of the interface as a function of time of the figures shown above.

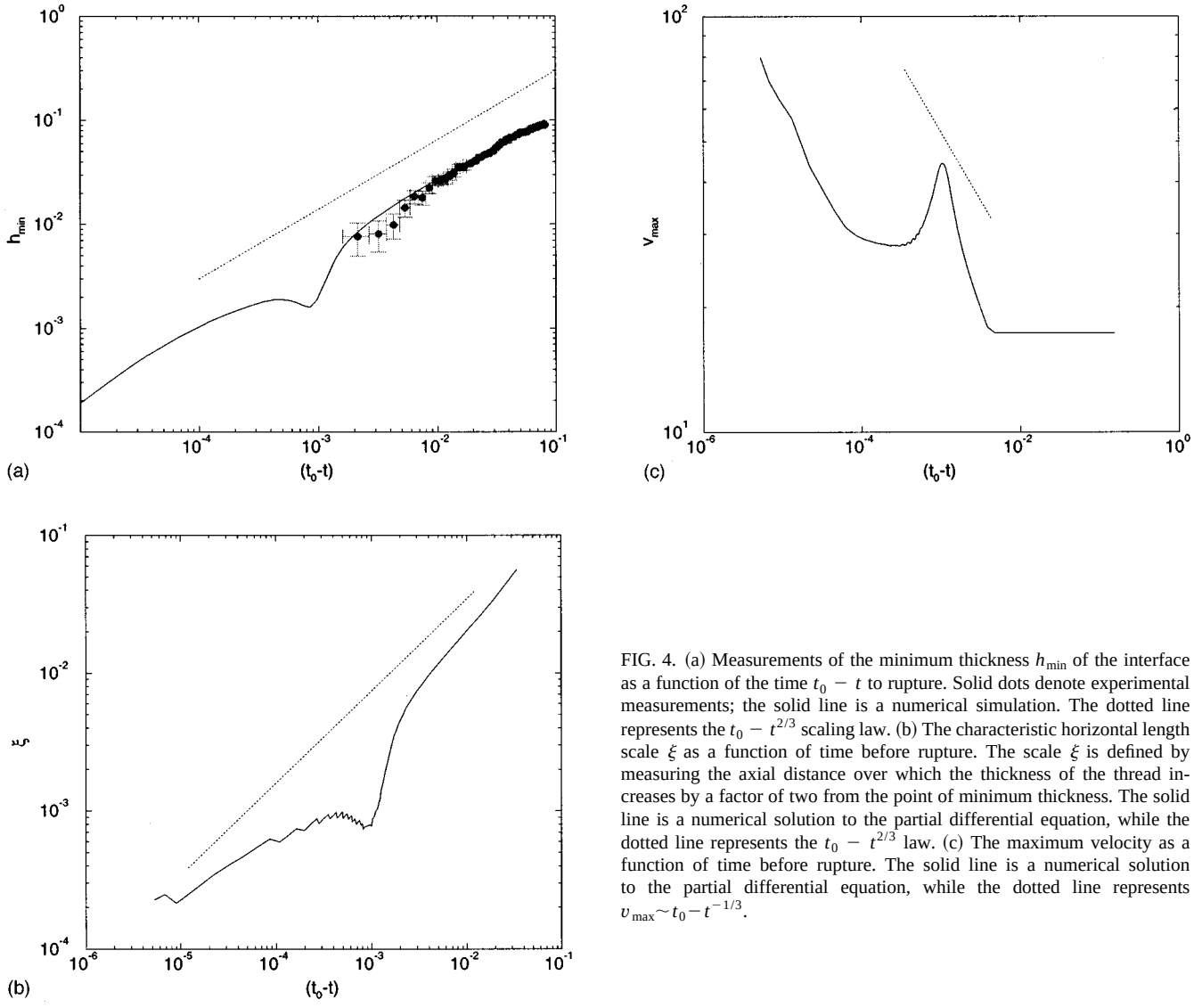

FIG. 4. (a) Measurements of the minimum thickness $h_{\min}$ of the interface as a function of the time $t_0 - t$ to rupture. Solid dots denote experimental measurements; the solid line is a numerical simulation. The dotted line represents the $t_0 - t^{2/3}$ scaling law. (b) The characteristic horizontal length scale ξ as a function of time before rupture. The scale ξ is defined by measuring the axial distance over which the thickness of the thread increases by a factor of two from the point of minimum thickness. The solid line is a numerical solution to the partial differential equation, while the dotted line represents the $t_0 - t^{2/3}$ law. (c) The maximum velocity as a function of time before rupture. The solid line is a numerical solution to the partial differential equation, while the dotted line represents $v_{\max} \sim t_0 - t^{-1/3}$.

Figure 4(a) shows $h_{\min}(t)$ for the second breaking event for both theory and experiments shown in Fig. 4. The minimum thickness was measured in units of the drop radius R, and the time was measured before to the singular time t_0. In simulations the singular time could be measured exactly. Experimentally it could be measured to within one frame of the movie corresponding to a time error of $\pm\ 2.5\times10^{-5}$ s. Note that the time is measured in terms of the time scale given in (4) to facilitate comparison between simulations and experiments. As above, R denotes the radius of the nozzle. The absolute scale on the photographs was not directly measured, but was instead deduced by comparison with simulations. The simulations can also measure the characteristic length of the interface and the maximum fluid velocity as a function of time to rupture. These dependences are shown in Figs. 4(b) and 4(c).

Note that the viscous length scale is 4×10^{-6} in dimensionless units, far below the scales shown.

Does this numerical data agree with the dimensional scaling law? There are two separate points to make: The experiments can resolve 2.5×10^{-5} s before the rupture, corresponding to $t_0-t\approx10^{-3}$. Before $t_0-t\sim10^{-2.5}$ simulations show a decrease of the minimum thickness consistent with the $t^{2/3}$ law; however, the simulation shows that a drastic event occurs near this time ΔT_E, causing a severe deviation from the scaling law. This event can be seen in all simulated quantities. Examining the experiments with this result in mind, there also seems to be a slight deviation of the data from straight power-law behavior around $t_0-t\sim5\times10^{-3}$, though it is difficult to establish this conclusion definitively with current resolution. (We remark, however, that we were unable to get rid of the slight ''glitch'' in the experimental time dependences near the breaking point by adjusting the time of rupture t_0. This is consistent with our conjecture that the deviation from power-law behavior is a real effect.)

We will discuss the physical origin of this behavior below. It is demonstrated that the time ΔT_E at which the deviation from $t^{2/3}$ occurs is *independent* of the viscosity of the fluid; for a fluid of viscosity ten times smaller than that of water the deviation also begins near $t_0-t=10^{-3}$. Thus, the scaling range does not become larger as the Reynolds number $\mathrm{Re}\to\infty$. This indicates an intrinsic failure of the dimen-

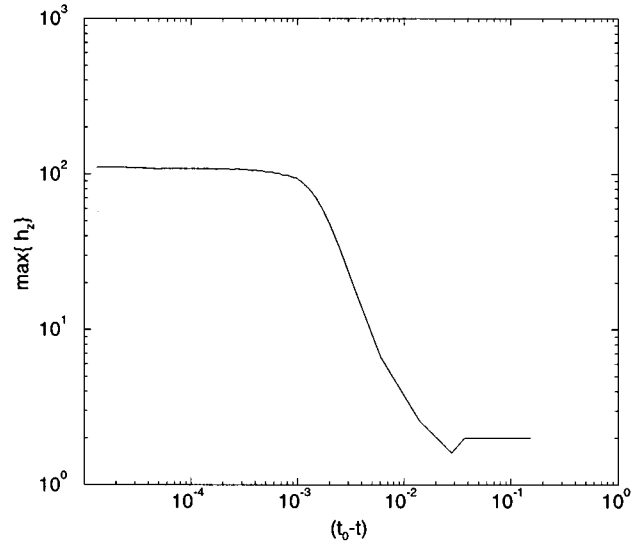

FIG. 5. The maximum slope of the interface as a function of time to rupture from simulations. The similarity solution equation (6) predicts that this slope should be constant in time.

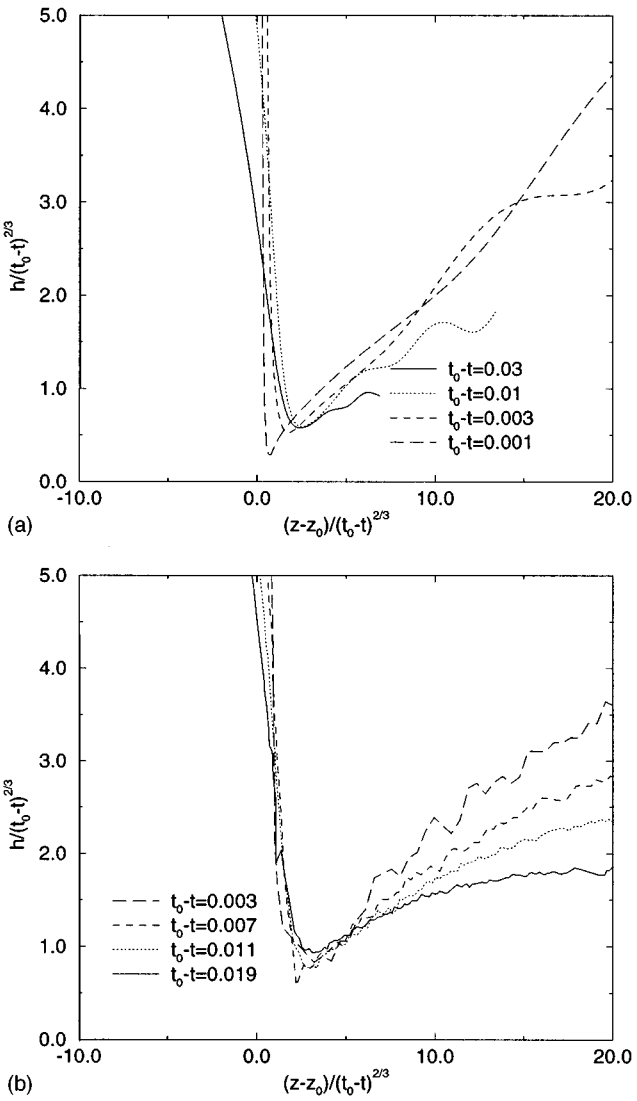

FIG. 6. (a) Rescaled profiles from numerics before the curvature singularity ($t_0-t \geqslant 10^{-3}$). Both horizontal and vertical scales are rescaled by $(t_0-t)^{2/3}$. The location of the final breaking point z_0 is subtracted from each of the profiles. The solid, dotted, dashed, and long dashed lines represent $t_0-t=0.03$, 0.01, 0.003, and 0.001, respectively. (b) Collapsed profiles from experiment. The location of the final breaking point z_0 is subtracted from each of the profiles. The solid, dotted, dashed, and long dashed curves represent $t_0-t=0.019$, 0.011, 0.007, and 0.003, respectively. Note that these experimental profiles show no evidence of overturning.

sional scaling argument, which suggests that the agreement between the $t^{2/3}$ law and experiments is somewhat artificial. Also, below, we present further experimental evidence for the breakdown of the assumptions leading to the dimensional scaling law, based on the shapes of the profiles.

What is the reason for the complex time dependence? It is counterintuitive that the minimum thickness does not decrease monotonically as the drop breaks, but actually *increases* for a short time. The origin of this can be understood by carefully examining the shape profiles: Figure 5 shows the maximum slope of the profile as a function of t_0-t: The inviscid similarity solution predicts that the slope should be constant. Before the nonmonotonic glitch, during the time period when the scaling laws are consistent with the dimensional scaling laws, the slope is constant [$\max(h_z)\approx 2$]; however, at $t_0-t\approx 10^{-2}$ the slope increases rapidly, saturating to a constant value [$\max(h_z)\approx 110$].

The major consequence of the time dependence of the slope is that when the profiles are rescaled according to Eq. (6), the shapes do *not* collapse on the steep side of the profile, as shown in Fig. 6(a). Thus, even though the time dependences agree with the dimensional predictions, the shapes are not self-similar in time, even before $t_0-t\approx 10^{-3}$, when the time dependence seems to agree with the dimensional scaling laws.

This same behavior can be seen in experiments [Fig. 7(b)]: Profiles were extracted from the images using the image processing package IDL, and then rescaled as outlined above: both radii and horizontal length scales are scaled by the characteristic length $l(t')$. The experimental profiles also do not collapse onto a single curve, implying that the dynamical behavior deviates from the similarity solution equation (6). Qualitatively, the experimentally collapsed profiles [Fig. 7(b)] are very similar to the simulations [Fig. 7(a)].

It is interesting to note that simulations of inviscid, irrotational flow[12,37] show an overturning of the profile at a finite time away from the singularity, rather than a gradual steepening. A profile that has overturned looks perfectly flat when viewed from the side, as done in the experiments. The fact that the simulations and experiments agree so well before breakup provides evidence that no such overturning occurs before breakup. As remarked before, the situation is different during violent satellite drop oscillations, where flat portions appear at the end of a drop.

The interfacial shapes in both simulations and experiments are inconsistent with the similarity solution (6). Although the characteristic length scales do agree with the similarity solution over a range of scales, the agreement breaks down in a regime where the similarity solution should still hold. Again, we emphasize that simulations with even smaller viscosity show that the deviation from the scaling

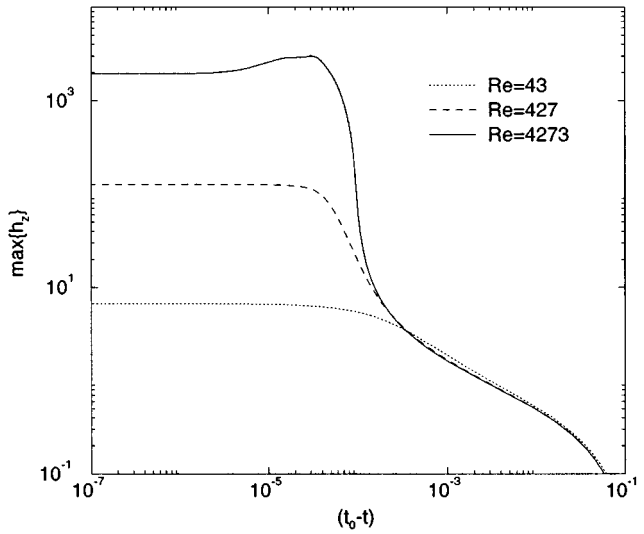

FIG. 7. Maximum slope during the course of a simulation as a function of time for liquid bridge simulations, for various Reynolds numbers. A liquid bridge is a cylinder of fluid held at constant radius at both ends.

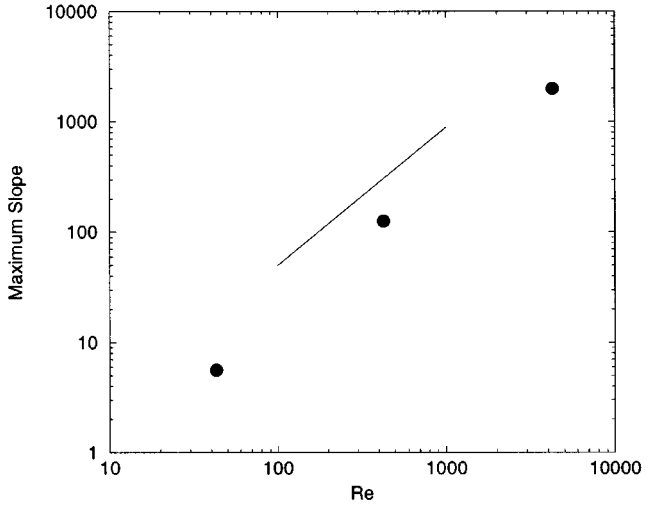

FIG. 8. Maximum slope as a function of Reynolds number, extracted from the liquid bridge simulations of Fig. 7.

solution occurs very near the time the deviation occurs above, so that the deviation is *not* a consequence of the finite fluid viscosity.

A. The curvature singularity

The overall deviation from self-similarity occurs because the slope next to the breaking point grows by a factor of 50 on a time scale much faster than the pinching. This steepening is a remnant of a finite time singularity in the *inviscid* equations; without viscosity, steepening leads to a singularity in which the local gradients in the velocity blowup in finite time. The mechanism of the steepening is a convective instability: regions of high velocity are convected at higher velocities, leading to a singularity in which the velocity gradient diverges with the velocity remaining finite. This points to the dynamical formation of a new length scale l_{Euler}, which approaches zero in finite time. The mechanism is reminiscent of shock formation in compressible hydrodynamics. For fluids with finite viscosity, the convective instability is stopped before $l_{\mathrm{Euler}} \to 0$, at a scale $\tilde{l}$ set by the viscosity. The length $\tilde{l}$ controls the maximum steepness of the front. This mechanism therefore provides a natural explanation for why low-viscosity fluids have very sharp fronts.

The maximum slope of the sharp front is controlled by the dynamics of the steepening. If the inviscid or Lee's equations are simulated, rapid growth occurs at the highest wave numbers, and the solution is dominated by fluctuations on the scale of the grid. Therefore, we performed a series of simulations at increasing Reynolds numbers, which we later extrapolate to the inviscid case. Even for the largest Reynolds numbers, no high-wave number instability was observed. Figure 7 plots the maximum slope for the Reynolds numbers Re=43, 427, and 4273 as a function of the time to rupture. All of the plots demonstrate a rapid increase in the slope up to a saturation level determined by the Reynolds number, similar to Fig. 5.

Finally, we note that the simulations depicted in Fig. 7 were done for a liquid bridge (a finite cylinder of fluid pinned at both ends) instead of drops falling from a faucet; the major differences are the absence of gravity for the liquid bridge, and the different initial conditions for the two cases. Although the basic qualitative features of the formation of the curvature singularity are independent of experimental configuration note that there are several quantitative differences between the dynamics of Fig. 7 and Fig. 5: the jet simulations have a different early time transient than the drop simulations. Also, at the highest Reynolds number (Re=4273), the jet simulation shows a nonmonotonic behavior. We do not know if this nonmonotonic behavior persists when $\mathrm{Re} \to \infty$. There are two important qualitative features of Fig. 7: first, the maximum slope *diverges* as the Reynolds number $\mathrm{Re} \to \infty$. Figure 8 plots the maximum slope as a function of Reynolds number for the above simulations.

The points are numerical data, and the solid line represents the scaling law

$$\max h_z \sim \mathrm{Re}^{1.25}. \tag{10}$$

We cannot be sure, however, that this exponent represents the asymptotic scaling law. Note that Re=4273 represents a fluid with one-tenth the viscosity of water, falling from a 1 cm nozzle. At the point where the slope reaches its maximum, the smallest features resolved are of the size 10^{-7}, which is the best we can do with the present numerical simulations.

The second important point is that the time at which the steepening begins is roughly independent of Reynolds number. Therefore, we conclude that the steepening is a remnant of a finite time singularity in the inviscid equations, in which the interfacial curvature diverges. This ''curvature singularity'' is distinct from the singularity at rupture, and introduces a new length scale into the problem a finite time from the rupture. This is the reason that the dimensional scaling laws break down before rupture. Moreover, the inviscid equations are not able to describe the bifurcation of a liquid drop, as the curvature singularity provokes a breakdown of the equations before breakup occurs.

As a word of caution, we reiterate that our theoretical description was based on an equation that has not been derived from the Navier–Stokes equations; moreover, the formal motivation for the equations breaks down in the limit of sharp slopes. The argument that we are making is that (1) the lubrication equations show this curvature singularity; (2) the solutions of the lubrication equations agree quantitatively with experiments, and therefore (3) it appears that the full equations must also show a curvature singularity in the inviscid limit, of the type described here. The actual structure (e.g., time dependences) of the singularity in the full Euler equations may be different than the structure in the lubrication equations.

B. After the curvature singularity

After the curvature singularity is stopped by viscosity, what is the resulting dynamics? This is a regime where we only have simulational evidence. Since the curvature singularity occurs at a time independent of Re, in principle as $\mathrm{Re}\to\infty$, there could be a large scaling region for another scaling solution. One possible scenario is that viscosity is only important in a thin boundary layer region, where it sets the maximum slope. In the other parts of the solution, viscosity is not important until the minimum thickness crosses the viscous length scale. Depending on how strongly the two parts of the solution affect each other, Keller–Miksis scaling could be observed.

Although the simulation above does seem to follow a $t^{2/3}$ law in the maximum velocity after the curvature singularity, the scaling of the other quantities behaves differently. Moreover, the profiles in this regime do not collapse upon rescaling. We take this as a hint that immediately after the curvature singularity there is a transient regime in which no scaling occurs. Neither our numerical simulations nor our experiments are able to resolve what happens after transients settle down, so that we are not able to determine the structure of the solution in this asymptotic regime.

We remark that Chen and Steen have recently carried out an interesting study[40] of the dynamics of a membrane with surface tension surrounded by an inviscid fluid. Their study shows a regime before rupture similar to that shown here, where the interfacial shape is single valued and the $t^{2/3}$ breaks down. However, in their example, the subsequent dynamics is quite different than that described here: Notably, in their case, the interface overturns before pinch-off (becomes double valued). After overturning, the dynamics eventually returns to the $t^{2/3}$ scaling. We believe that the difference between the two studies is that in the present study the curvature singularity is regularized by viscosity, which stops the steepening of the slope and prevents overturning. However, more work on the limit of infinite Reynolds number in the full Navier–Stokes equation is necessary.

V. SHAPES AFTER RUPTURE

Immediately after rupture, the shape of the interface on the length scales of the experimental photographs [Fig. 4(b)] looks like a sharp conical tip attached to a spherical shell. A conical tip has no intrinsic length scale, and thus should recoil according to the $t^{2/3}$ scaling law. Measurements of how this sharp tip relaxes after the rupture can be extracted from both experiments and simulations, in the same manner as outlined above. There are two dynamical length scales of interest: the length $L(t)$ that the tip has recoiled a time t after the rupture, and the characteristic thickness $w(t)$ of the neck. Simulations can also measure the velocity v_{tip} of the recoiling tip. Figure 9 shows plots of these quantities from both experiments [Fig. 9(a)] and simulations [Figs. 9(b) and 9(c)]. We remind the reader that the rupture time used for this figure is exactly the same time as the one used for the analogous plots before breakup. Thus, given the rupture time determined before breakup, the plots after breakup contain no free parameters.

Although the experimental data seems to be consistent with the dimensional scaling laws, in the simulations there are rather severe deviations, especially very close to the rupture time. It should be noted that the deviations from the dimensional scaling law occur when the droplet thickness is far greater than the viscous length scale. The basic question is whether the deviation of the simulations from the dimensional scaling law represents a *fundamental* or if it merely reflects a breakdown of the approximations within the simulations.

The reason for the breakdown in the scaling laws for the simulations can be understood by examining the shape of the interface immediately at the point of rupture, before any recoiling occurs (Fig. 10). Recall that the experimental shapes, as shown in Fig. 4(b), show a conical tip before the recoiling.

The simulations can probe much closer to the breaking point than the experiments. It is clear from Fig. 10(a) that the shape at the instant of rupture in the simulations is more complicated than a simple conical tip (though at large scales the shape does look conical). The region bracketed in the figure between $0.83<z<0.91$ is conical, though there are transitions to different shapes on both sides of this region. Figure 10(b) shows a closeup of the region on the left-hand side of the conical tip, nearest to the breaking point.

The closeup reveals *another* conical region between $0.795 < z < 0.8$, and also a crossover to a more slender region near $z=0.795$. The complicated structure of the interface at the rupture point is a remnant of the dynamics before breakup. The crossover at $z=0.795$ noted in Fig. 10(b) arises from the curvature singularity before breakup, and corresponds roughly to the interfacial thickness ($h_{\mathrm{min}}\approx 10^{-3}$), where the curvature singularity saturates (see Fig. 6). The crossover between the two conical regions near $z=0.83$ occurs when the recoiling tip interacts with the capillary waves caused by the recoiling of the first rupture at the bottom of the neck [see Fig. 4(a)].

The argument of Keller[29] based on mass and momentum conservation of the recoiling tip (see Appendix C) shows that the time dynamics of recoiling reflects the detailed structure of the initial shape. If the initial shape is a power law, then the time dependences are power laws; Given the complicated initial shape in the present situation, we expect the time dynamics after breakup to be more complicated than a simple scaling law, with crossovers corresponding to the crossovers in the initial shape.

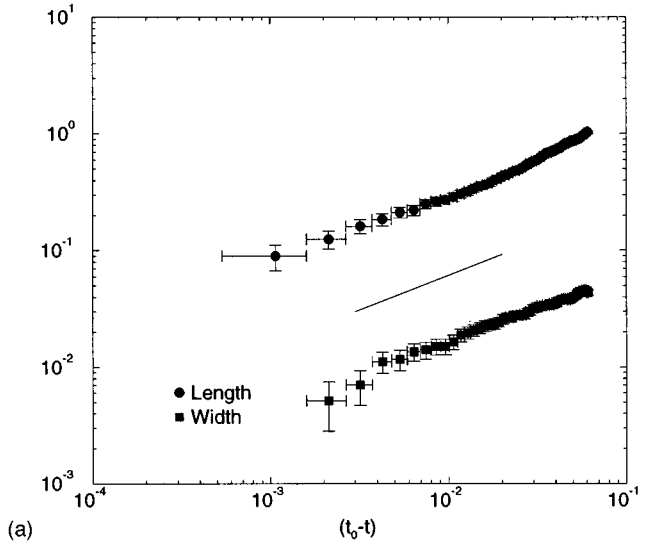

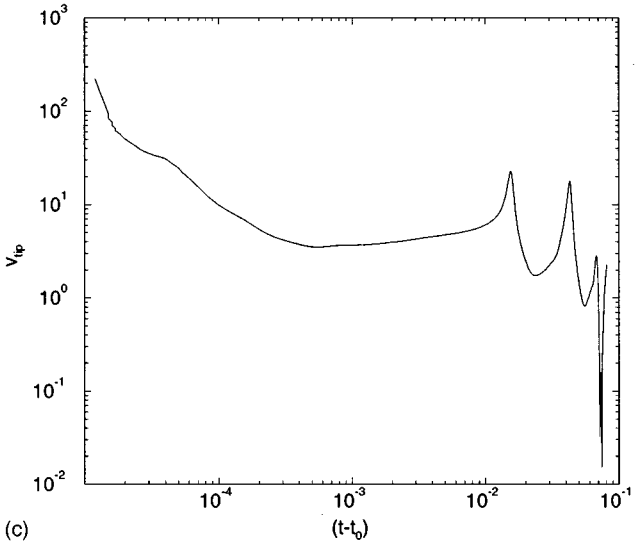

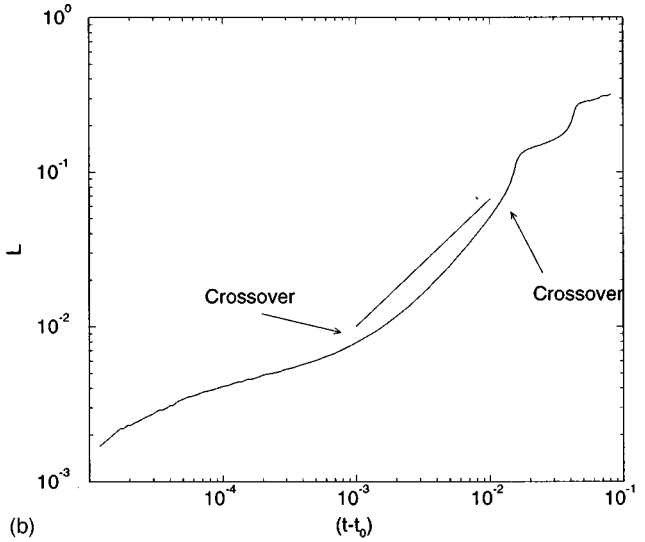

FIG. 9. (a) Recoil length and width as a function of time measured from experiments. Distances are measured in units of R. The recoil length is shifted vertically by a factor of 10. The solid line represents the $(t_0-t)^{2/3}$ scaling law. (b) Plot of the recoil length as a function of time from simulations. The solid line corresponds to the Keller–Miksis scaling law $(t_0-t)^{2/3}$. (c) Plot of velocity of the recoiling tip as a function of time from rupture in simulation.

Indeed, the two crossovers noted in the time dependences of Fig. 9(b) to the crossovers in the initial shape. The first crossover, occurs when the recoil length is 10^{-2}, and corresponds to the crossover noted in Fig. 10(b). The second crossover occurs when the recoil length is around 2×10^{-1}, and corresponds to the large-scale crossover in Fig. 10(a). These crossovers are also apparent in the scaling for the tip velocity v_{tip}. There does exist a region on the plot of the recoil length where the time dependence is well approximated by the $t^{2/3}$ law. This region, between $t_0-t\approx10^{-3}$ and $t_0-t\approx2\times10^{-2}$ occurs nearly at the same time that the experiments show time dependences consistent with the Keller–Miksis laws (Fig. 9). The ''wiggles'' appearing in the simulations at times larger than $t_0-t>2\times10^{-2}$ do not seem to exist in the experimental data [Fig. 9(a)]; this seems to represent a quantitative discrepency between the experiments and the simulations. To substantiate that the ''wiggles'' arise from the interaction of the recoiling neck with capillary waves in the initial shape, we have studied the time dynamics of recoiling at the bottom of the neck [Fig. 3(a)]: in this case, the crossover due to the curvature singularity still occurs at the same characteristic thickness, while the crossover at large scales is completely absent, as no capillary modulations exist before the recoiling. It should also be noted that Fig. 9(c) is completely inconsistent with the dimensional scaling law $t^{-1/3}$, even in the range where the length is roughly consistent with the dimensional scaling law.

As mentioned in our description of the dynamics before breakup, a more precise test for whether the scaling hypothesis is realized is to collapse the profiles by their characteristic length scales. Because of the complications outlined above we focus on only the regime where scaling occurs. Figure 11(a) shows the interfacial profiles after rupture from the simulations, rescaled according to Eq. (6), for several different times after the rupture.

A similar procedure can be applied to the experimental data, as shown in Fig. 11(b). The data collapse reasonably well, although only over a finite range in similarity variables. The reason for this is twofold: First, there are finite size

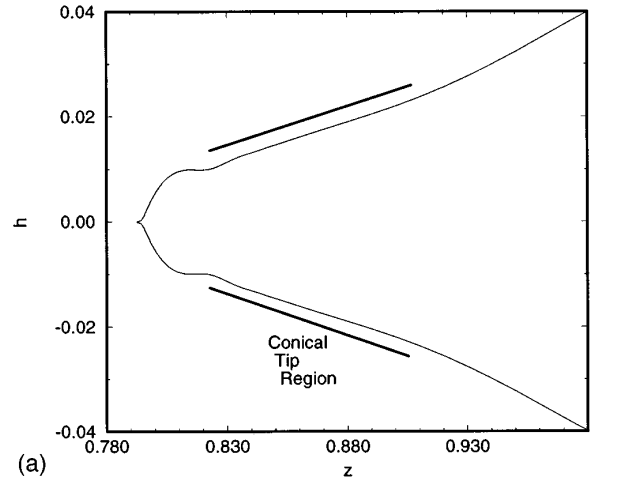

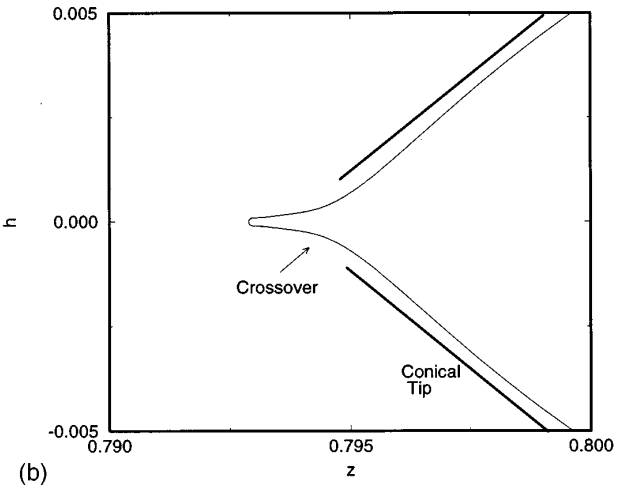

FIG. 10. (a) Shape of the interface *a* the instant of rupture from numerical simulations. Because the shape is not a power law, the argument of Keller (see Appendix C) suggest that the time dependences will not be perfect power laws. (b) Closeup of (a) of the initial shape of the interface before recoiling.

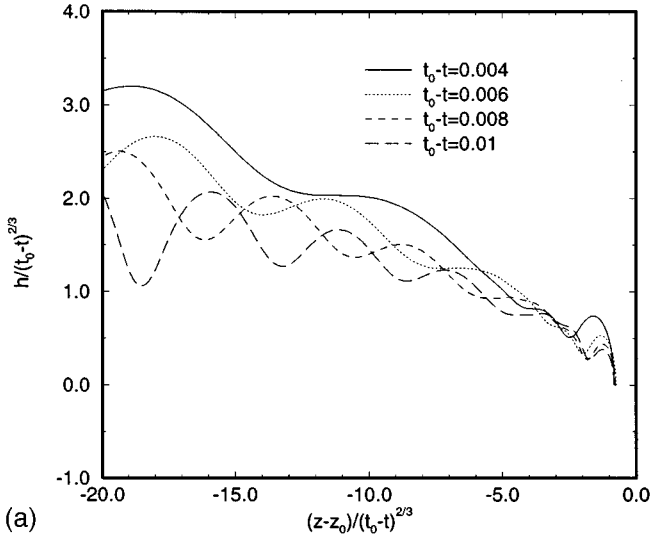

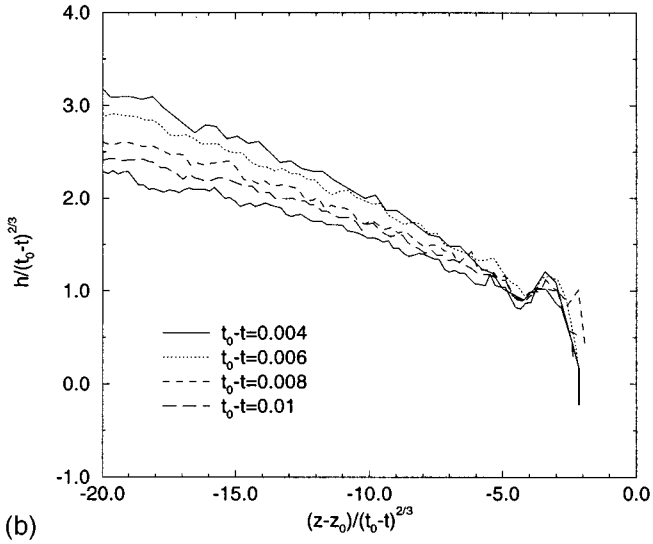

FIG. 11. (a) Collapsed solutions from simulations for the recoiling fluid neck. (b) Collapsed solutions from the experiment. Length scales are measured in pixels from the photographs.

effects associated with the neck having a finite length and observations being made a finite distance away from the singularity. The second reason is the initial shape is not a pure power law, and this causes deviations.

In Appendix C we show a simulation that *does* start out with a conical initial shape, and show that it is perfectly described by the Keller–Miksis scaling theory. This validates the argument of this section that the deviations from the Keller–Miksis scaling law are not because of a dynamical instability but instead complications in the initial shape.

VI. CONCLUSIONS

Experiments demonstrate that the shape of a fluid displays a dramatic dependence on fluid viscosity (cf. Fig. 1). Whereas high-viscosity fluids are slender near the breaking point, water drops exhibit a sharp conical tip. In this paper we have presented detailed comparisons between experiments and numerical simulations of the breaking of low-viscosity fluid drops, in order to understand better the dynamics at low viscosity. The simulations are of one-dimensional evolution equations that were previously derived by several groups[24,30] using asymptotic analysis from the Navier–Stokes equations. In Appendix A we present an alternative way of looking at the equations emphasizing symmetries and conservations laws. The version of the equations employed here uses an approximation of the mean curvature that captures the exact equilibrium shapes of pendant drops. Because of this, the numerical simulations and experiments are in quantitative agreement well beyond the initial fission event. We present a series of two experiments and simulations, demonstrating the excellent agreement between simulations and experiments throughout the breaking process.

Detailed comparisons between the dynamics of the simulations and the experiments uncovered several intrigu-

ing features of the dynamics of low-viscosity fluid drops. In this study we demonstrate the presence of a *convective instability* of the drop shape before breakup. The dynamics of the instability is reminiscent of shock formation in gasdynamics, and occurs because regions of high fluid velocity are convected faster than low-velocity regions. This instability is stopped by viscous stresses; in this way viscosity sets the *scale* for the steep tip in water drops. The convective instability reflects that the infinite Reynolds number limit is singular: the convective instability forces equations with $\mathrm{Re}=\infty$ to develop a finite time singularity well before the drop breaks. With very small viscosity, the sharp tip forms on a very fast time scale well before rupture, though the first bonafide singularity occurs at rupture. An intriguing consequence of the formation of a sharp tip is that for fluids with viscosity much smaller than water, so that the viscous length scale is smaller than the molecular length scale, the convective instability is actually regularized by molecular effects instead of viscous dissipation: in this case, the hydrodynamic equations break down well before the drop itself breaks.

In this study we provide a concrete example of the complications that can occur in describing a singularity. Although dimensional arguments and their corresponding similarity solutions are suggestive, in general whether they are actually realized depends on subtle dynamical issues, which at present are not entirely understood. Instabilities of scaling solutions in the limit where dissipation approaches zero might be important in other contexts where singularities occur in inviscid flows, such as the three-dimensional Euler equation. An example of of a basic issue that we still do not understand is why the system chooses the similarity solution in Eq. (7) with $\beta=1$ before breakup, corresponding to the Keller–Miksis scaling law. In principle, any value of β could have occurred, and would have caused both different time dependences and different interfacial shapes away from the breakup point. Although our study confirms that there is something special about the similarity solution suggested by dimensional analysis, we do not understand the dynamical mechanism that selects this solution. Perhaps selection principles, analogous to those used previously in resolving similar issues for traveling wave solutions[41] are relevant for the formation of singularities.

On a different level, this study provides another step toward understanding the dynamics, leading to the breaking of a fluid drop. The general picture emerging is that rupture is described by a number of different scaling regimes; The particular state of the drop is controlled by dimensionless parameters formed by combining fluid parameters with length scales characterizing the drop. Since the latter are time dependent, a drop typically passes through several different scaling regimes during a single fission event. Understanding the details of each scaling regime individually, and when the various crossovers occur, yields a quantitative description of the breaking dynamics.

ACKNOWLEDGMENTS

We thank Dan Mueth and David Grier for assistance with writing the image processing programs used to extract the profiles from the experiments. We are also grateful to the referees, both for their insightful comments, and for their patience during the review process.

This research was partially supported by the MRSEC Program of the National Science Foundation under Award No. DMR-9400379. In addition, M.P.B. acknowledges a National Science Foundation postdoctoral fellowship, and the Sloan Fund of the School of Science at MIT. J.E. acknowledges support by the Deutsche Forschungsgemeinschaft through Sonderforschungsbereich 237.

APPENDIX A: DERIVATION OF LUBRICATION EQUATIONS

In this appendix, we motivate the nonlinear evolution equations by relying on conservation laws and symmetries of the full equations. Our principle aim is to emphasize that the long wave equations are the simplest one-dimensional partial differential equations that could be expected to model the motion of a droplet. The discussion is similar to the previous work of Green,[35] whose theory was applied by Shield *et al.*[42] The first equation that the fluid must satisfy is mass conservation:

$$(h^2)_t=-(h^2v)_z, \tag{A1}$$

where $h(z,t)$ is the thickness of the fluid neck an axial distance z from the nozzle, and $v(z,t)$ is the azimuthal component of the velocity. As in the main text, we nondimensionalized lengths by the nozzle radius R, and times by $\sqrt{\rho R^3/\gamma}$. Galilean invariance implies that the equation of motion is of the form

$$v_t+vv_z=-\kappa_z+D, \tag{A2}$$

where κ is the curvature and D is the dissipation function. A general form for D and p follows from the requirement that the total energy,

$$E=\int dz\ h^2v^2+\int dz\ h\sqrt{1+h_z^2},$$

satisfies $\partial_t E<0$. This implies that $p=\delta E/\delta h$, and that D is of the form

$$D(h,v)=\frac{1}{h^2}\left[-f_1v+(f_2v_z)_z-(f_3v_{zz})_{zz}+(f_4v_{zzz})_{zzz}+\cdots\right],$$

where the f_i are positive definite functions of v and h. The values of the f_i can be obtained to leading order by *demanding* that the model equations exactly reproduce the linear growth rate of the full hydrodynamic equations. For the case of present interest, liquid falling into vacuum, this implies that $f_1=0$ and $f_2=3/\mathrm{Re}$.

Thus, the equations are

$$(h^2)_t=-(h^2v)_z, \tag{A3}$$

$$v_t+vv_z=\frac{3}{\mathrm{Re}\ h^2}(h^2v_z)_z-\kappa_z, \tag{A4}$$

$$\kappa = \left(\frac{1}{h\sqrt{1+h_z^2}} - \frac{h_{zz}}{(\sqrt{1+h_z^2})^3} \right), \tag{A5}$$

where Re is Reynolds number.

The most important point of this argument is that the model equations are constructed so as to dissipate the *total* energy of the fluid while preserving the *exact* dispersion relation of linear disturbances, in the long-wavelength limit. This means that the model is guaranteed to predict exactly the correct equilibrium shapes of the theory, as well as the correct linear disturbances for modulations about a cylinder.

APPENDIX B: NUMERICAL CONSIDERATIONS

The numerical simulations utilize a second-order centered finite difference scheme of the partial differential equations (1)–(3), which has been previously described in several places. The goal of this appendix is to mention the various pitfalls and tricks that were necessary to develop for the simulations reported in this paper.

There were two different numerical challenges: the first involved issues associated with breaking the drop and simulating the subsequent dynamics (Figs. 2 and 3). *A priori* it was unclear that these simulations would work because of the concerns about overturning expressed in the main text, and demonstrated in completely inviscid simulations. It was also necessary to develop algorithms to deal with the simulation of many drops simultaneously.

The second numerical challenge was to resolve the various singularities described in this paper. We emphasize that in order to achieve enough numerical data to make accurate assertions about singularity mechanisms, it is necessary to have *at least* several decades of power law behavior. Without several decades of scaling, it is possible to be fooled in two possible ways: first convergence to similarity solutions does *not* occur exponentially in time, but instead exponentially in $-\log(t_0-t)$. This means it typically takes a few decades of scaling for the transients to die out and reveal the true scaling behavior. Without several decades of scaling measurements of exponents will be inaccurate; the latter can be self-consistently tested by determining if the solution converges to the spatial structure of the similarity solution. Second, recent work[23] has demonstrated that there are concrete physical examples of singularities which can destabilize at arbitrarily small time distances from singularities. Although this can never be ruled out completely in a purely numerical study, a sufficiently large number of decades of scaling makes this outcome less probable.

Before proceeding into specific issues that arise with each of these problems, we first summarize some of the general procedures. The time step control was adjusted so that only one Newton iteration was required at each time step. The time step is adjusted by using a two step method: for each time step, we first step by Δt, and then redo the calculation with two time steps of size $\Delta t/2$. The relative error in the solution is then computed. Typically the time step is controlled by demanding that the relative error is less than a fixed threshold (e.g., 1%).

High resolution is achieved by using a dynamically adjusting mesh. At low viscosities there are two different singularities: one associated with the minimum height going to zero, the other with diverging gradients. Thus we monitored both the minimum height and the gradient of the mass flux $h^2 v$. If either changed by a specified percentage, new mesh points were added to the grid. The mesh is organized by defining an underlying macrogrid, and adjusting the number of microgrid elements into which each macrogrid is divided. After introducing new grid points, the solution is reinterpolated onto the new grid. Typically linear interpolation or cubic splines are used.

A subtlety of this procedure is that at places where the mesh spacing changes by a factor of 2, we observed an instability of the discretized equations. This may be connected with the fact that our spatial discretization was only first order correct at those places (because of the h_{zzz} term at the mesh points). This ''numerical noise'' does not have a large effect on highly viscous fluids, though it is capable of initiating instabilities in viscous similarity solutions. However, as $\mathrm{Re}\to\infty$ these effects are quite substantial and make accurate numerical simulations very difficult. In order to perform the simulations at the highest Reynolds numbers, it was necessary to *smooth* the mesh. This was done by diffusing the mesh points until the ratio of neighboring mesh spacings differed by less than a percent.

To break a drop, we used the following procedure. A threshold thickness h_{thres} was defined (typically 10^{-5}). When the minimum thickness of the fluid neck passes below h_{thres} the drop is manually broken into two pieces, by attaching small spherical masses of fluid to each end. The radius of the spherical masses was determined by demanding that it has constant pressure. The interpolation of the spherical mass onto the fluid was done so that h_{zz} is continuous. Extensive tests revealed that the macroscopic dynamics was insensitive to both the precise spatial location of the breaking point as well as h_{thres}.

Once the drop was broken, each of the drops remaining were evolved by the code. The thickness h_i, the velocity v_i, and the positions z_i of each point were stored and the equations of motion applied at each time step. Regridding proved to be crucial for following through many ruptures, in order to always have enough mesh points.

APPENDIX C: IDEALIZED INITIAL CONDITIONS: CONES AND CUSPS

We have seen that simple theories based on a rescaling of the pinch region are invalidated by the appearance of another singularity, which introduces a second length scale not directly associated with the pinch. This inviscid singularity is convective in character, and thus arises through the mass flux across the pinch region. After breakup, this mechanism is absent, because the flow across the pinch region is interrupted. Hence it seems as if self-similar solutions should exist after breakup. However, it turns out that the solution after breakup depends heavily on the shape of the interface $h_0(z)=h(z,0)$ at breakup, which in turn is a reflection of the

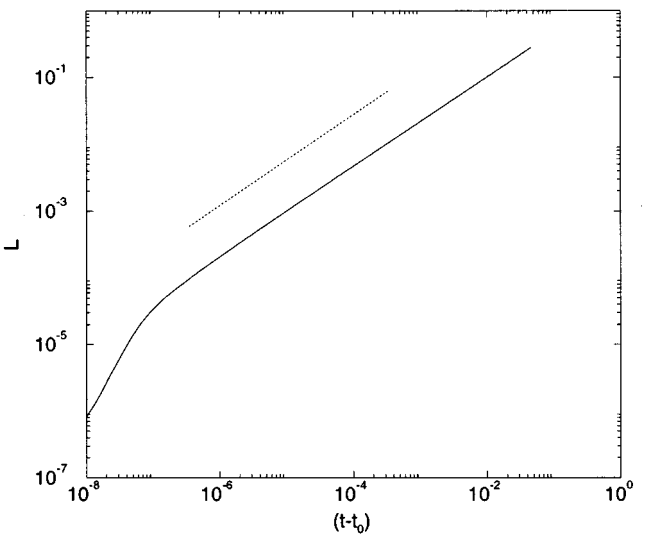

FIG. 12. Time dependences for the recoiling length L as a function of the time $t-t_0$ from the initial cone. The dots represent numerical data and the solid line is the Keller–Miksis scaling law. The crossover at $L \approx 10^{-4}$ corresponds to the small-scale cutoff in the initial condition.

dynamics *before* breakup. If additional length scales play a role before breakup, they are thus also introduced into the dynamics after breakup.

This is immediately evident from the arguments advanced by Keller[29] and worked out in more detail by Keller, King, and Ting,[43] using a matched asymptotic expansion. The first assumption is that velocities at breakup are small compared with the velocities produced by the violent recoil, so $h_0(z)$ is the only input needed. The second assumption, which was validated by the matching in Ref. 43, is that the fluid contained in the part of the neck that has already recoiled is sucked up into a spherical head. Intuitively, this is because there is no flux across the head, so it is accelerated uniformly by the recoil, and assumes a static shape. To a first approximation, one neglects the crossover region between the bulbous head and the static part of the neck, which has not yet recoiled. Thus, apart from $h_0(z)$, the geometry is completely specified by the recoil length $L(t')$ (which defines the head's center, with $t'=t-t_0$ the dimensionless time from the initial cone) and the width of the head $w(t')$. Figure 12 shows the time dependences from a numerical simulation of a recoiling cone. The initial shape is conical with a small spherical cap of size h_0, so that $L(0)$ and $w(0)$ are of order h_0. The time dependences agree quite well with the Keller–Miksis scaling law, except for a small transient period of order $\sqrt{h_0^3\rho/\gamma}$ (in dimensional units).

Mass conservation gives

$$\frac{4\pi}{3}\, w^3 - \pi \int_0^L h_0^2(z)\,dz = 0, \tag{C1}$$

and from conservation of energy we have

$$\frac{2\pi}{3}\, w^3 L_t^2 + \left\{ 4\pi w^2 - 2\pi \int_0^L h_0 \sqrt{1+h_{0z}^2}\,dz \right\} = 0. \tag{C2}$$

To exemplify the dependence of the solution on h_0, we assume that

$$h_0(z) = bz^\beta, \quad \beta \geqslant 1, \tag{C3}$$

as was done by Ting and Keller.[39] We hasten to add that a self-similar solution with $\beta \neq 1$ was never observed experimentally or in simulations. The case $\beta=1$ was observed over a limited scaling range, whose size does not expand for decreasing viscosity. To focus on scaling properties, we assume that

$$w(t') \sim t'^{\alpha_1}, \quad L(t') \sim t'^{\alpha_2}. \tag{C4}$$

From (C1) one has

$$w \sim L^{(2\beta+1)/3},$$

and combining that with (C2) one obtains

$$\alpha_1 = \frac{2}{3}\left(\frac{2\beta+1}{\beta+2}\right), \quad \alpha_2 = \frac{2}{\beta+2}. \tag{C5}$$

Two crucial observations are to be made here: First, the solution explicitly depends on β, i.e., on the initial condition h_0. If h_0 does not scale like a power law, as it is observed in simulations, neither will w or L. Second, only if $\beta=1$, which corresponds to Keller–Miksis scaling, will the solution be describable by a single rescaling $\xi=z/L$ of the abscissa. Namely, for $\beta=1$ w and L both scale like $t'^{2/3}$, as to be expected from Keller–Miksis scaling, while for $\beta>1$ the two will scale differently. The time dependence of the neck length L agrees with the scaling law proposed by Ting and Keller,[39] which is based on the scaling ansatz (8), (9). However, the width of the tip w is in disagreement with this scaling for $\beta>1$. This is not surprising because the underlying assumption is that the slope h' is negligible, which evidently is not the case near the tip. Therefore, the solution must assume a more complicated structure, the neck and the tip region being governed by different scaling laws.

Finally, we discuss the case $\beta=1$ in a little more detail, since it can be understood completely within the framework of our simplified model (1), (2). It also gives the closest approximation to existing experimental data. Namely, in that case (6), (7) is an exact solution of the inviscid equations, if H and V obey the similarity equations

$$\begin{aligned} &\frac{2}{3}H - \frac{2\xi}{3}H' = -VH' - \frac{1}{2}V'H, \\ &-\frac{V}{3} - \frac{2\xi}{3}V' = -VV' + \left(\frac{1}{H\sqrt{1+H'^2}} - \frac{H''}{(\sqrt{1+H'^2})^3}\right)'. \end{aligned} \tag{C6}$$

Here the primes denote a derivative with respect to the similarity variable ξ. These equations have to be solved subject to two sets of boundary conditions. At infinity H and V should behave like

$$H = a\xi, \quad V = b\xi^{-1/2}, \tag{C7}$$

and at the tip, located at $\xi=\xi_0$, one has

$$H(\xi_0)=0, \quad H'(\xi_0)=\infty, \quad V(\xi_0)=\frac{2\xi_0}{3}. \tag{C8}$$

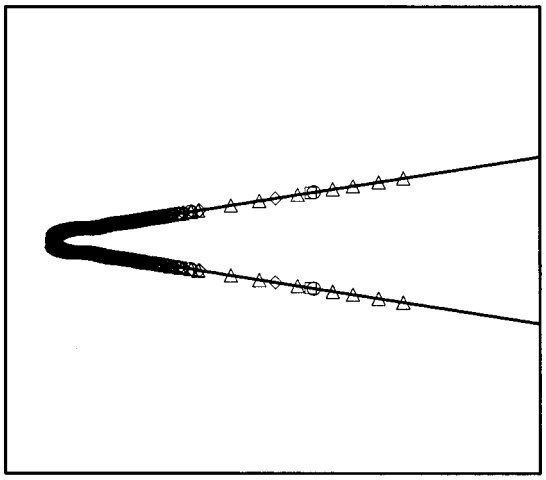

FIG. 13. Collapsed numerical data for the recoiling cones. Each of the symbols refers to numerical data, corresponding to the times 10^{-6} (circles), 10^{-5} (squares), 10^{-4} (diamonds), 10^{-3} (triangles), 10^{-1} (side triangles), and 50^{-1} (X) from the initial conical shape. The solid line is a similarity solution of the inviscid equations.

Two free parameters, which are the tip position and the velocity gradient $V'(\xi_0)$ at the tip have to be adjusted to make the solutions match the free constants a and b in (C7). This procedure is analogous to the one employed in Ref. 26 for *viscous* solutions.

In Fig. 13 a solution of (C6) is compared with the result of a simulation, starting from a perfect cone $h_0(z)=az$ and zero initial velocity. The value $a=0.13$ was chosen close to the opening angles observed in Fig. 3, while in experiments unfortunately b is not available. Among other things, the excellent agreement between simulation and the prediction of similarity theory shows that the small amount of viscosity present in the simulation does not appreciably affect the solution on scales $L \gg l_\nu$. Thus the viscous terms do not represent a singular perturbation, as was the case before breakup.

The similarity solutions also allow for an analytical understanding of the capillary waves excited on the surface, which are the most characteristic feature of inviscid solutions. Namely, repeating the perturbative analysis of Ting and Keller[39] for the model (1), (2), we find the amplitude and wavelength of capillary waves on the receding cone as a function of the parameters a and b. The wavelength just depends on a, reflecting the weak dependence of the solution on the initial velocity field:

$$\lambda = 2\pi \left(\frac{9}{8} \frac{a}{(\sqrt{1+a^2})^3} \right)^{1/2} \xi^{-1/2}. \tag{C9}$$

Thus the wavelength gets shorter farther away from the tip. The analytical formulas are confirmed beautifully by the simulation, but are difficult to observe experimentally, because of the shortness of the scaling range.

The same observation was made by Schulkes,[37] who simulated inviscid, irrotational flow. While solutions starting from initial cones collapse well under Keller–Miksis scaling, no quantitative collapse is found for initial shapes that came from his computations.

[1] J. Plateau, *Statique Experimentale et Theoretique des Liquides Soumis aux Seules Force Moleculaire* (Gauthier Villars, Paris, 1873).
[2] W. S. Rayleigh, ''On the instability of jets,'' Proc. London Math. Soc. **4**, 10 (1878).
[3] A. M. Worthington, *A Study of Splashes* (Longmans, London, 1908).
[4] H. E. Edgerton, *Stopping Time: The Photographs of Harold Edgerton* (Abrams, New York, 1987).
[5] E. A. Hauser, H. E. Edgerton, and W. B. Tucker, ''The application of the high-speed motion picture camera to the research on the surface tension of liquids,'' J. Phys. Chem. **40**, 973 (1936).
[6] H. E. Edgerton, E. A. Hauser, and W. B. Tucker, ''Studies in drop formation as revealed by the high-speed motion camera,'' J. Phys. Chem. **41**, 1017 (1941).
[7] R. J. Donnelly and W. Glaberson, ''Experiments on the capillary instability of a liquid jet,'' Proc. R. Soc. London Ser. A **290**, 547 (1966).
[8] E. F. Goedde and M. C. Yuen, ''Experiments on liquid jet instability,'' J. Fluid Mech. **40**, 495 (1970).
[9] D. F. Rutland and G. J. Jameson, ''A nonlinear effect in the capillary instability of liquid jets,'' J. Fluid Mech. **46**, 267 (1971).
[10] K. C. Chaudhary and T. Maxworthy, ''The nonlinear capillary instability of a liquid jet. Part 2: Experiments in jet behavior before droplet formation,'' J. Fluid Mech. **96**, 275 (1980).
[11] K. C. Chaudhary and T. Maxworthy, ''The nonlinear capillary instability of a liquid jet. Part 3: Experiments on satellite drop formation and control,'' J. Fluid Mech. **96**, 287 (1980).
[12] N. N. Mansour and T. S. Lundgren, ''Satellite formation in capillary jet breakup,'' Phys. Fluids A **2**, 114 (1990).
[13] H. A. Stone, B. J. Bentley, and L. G. Leal, ''An experimental study of transient effects in the breakup of viscous drops,'' J. Fluid Mech. **173**, 131 (1986).
[14] H. A. Stone and L. G. Leal, ''Relaxation and breakup of an initially extended drop in an otherwise quiescent fluid,'' J. Fluid Mech. **198**, 399 (1989).
[15] M. Tjahjadi, H. A. Stone, and J. M. Ottino, ''Satellite and subsatellite formation in capillary breakup,'' J. Fluid Mech. **243**, 297 (1992).
[16] P. Constantin, T. Dupont, R. Goldstein, L. Kadanoff, M. Shelley, and S. Zhou, ''Droplet breakup in the Hele-Shaw cell?,'' Phys. Rev. E **47**, 4169 (1993).
[17] T. Dupont, R. Goldstein, L. Kadanoff, and S. Zhou, ''Finite-time singularity formation in Hele–Shaw systems,'' Phys. Rev. E **47**, 4182 (1993).
[18] R. E. Goldstein, A. I. Pesci, and M. J. Shelley, ''Topology transitions and singularities in viscous flows,'' Phys. Rev. Lett. **70**, 3043 (1993).
[19] A. Bertozzi, M. Brenner, T. Dupont, and L. Kadanoff, ''Singularities and similarities in interface flow,'' in *Centennial Edition, Applied Mathematics Series* edited by L. Sirovich (Springer-Verlag, Berlin, 1993).
[20] D. H. Peregrine, G. Shoker, and A. Symon, ''The bifurcation of liquid bridges,'' J. Fluid Mech. **212**, 25 (1990).
[21] J. Keller and M. J. Miksis, ''Surface tension driven flows,'' SIAM J. Appl. Math. **43**, 268 (1983).
[22] G. I. Barenblatt, *Similarity, Self-Similarity and Intermediate Asymptotics* (Consultants Bureau, New York, 1979).
[23] R. Almgren, A. Bertozzi, and M. P. Brenner ''Stable and unstable singularities in the unforced Hele–Shaw cell,'' Phys. Fluids **8**, 1 (1996).
[24] J. Eggers and T. F. Dupont, ''Drop formation in a one-dimensional approximation of the Navier–Stokes equation,'' J. Fluid Mech. **262**, 205 (1994).
[25] J. Eggers, ''Universal pinching of 3d axisymmetric free-surface flow,'' Phys. Rev. Lett. **71**, 3458 (1993).
[26] J. Eggers, ''Theory of drop formation,'' Phys. Fluids **7**, 941 (1994).
[27] X. D. Shi, M. P. Brenner, and S. R. Nagel, ''Cascade of structure in a drop falling from a faucet,'' Science, **265**, 219 (1994).
[28] M. P. Brenner, X. D. Shi, and S. R. Nagel, ''Iterated instabilities during droplet fission,'' Phys. Rev. Lett. **73**, 3391 (1994).
[29] J. B. Keller, ''Breaking of liquid films and threads,'' Phys. Fluids **26**, 3451 (1983).
[30] S. Bechtel, M. G. Forest, and K. J. Lin, ''Closure to all orders in 1d models for slender viscoelastic free jets: An integrated theory for axisymmetric, torsionless flows,'' Stability Appl. Anal. Continuous Media **2**, 59 (1992).
[31] R. W. Sellens, ''A one-dimensional numerical model of the capillary instability,'' Atom Sprays **2**, 236 (1992).
[32] X. Zhang and O. A. Basaran, ''An experimental study of dynamics of drop formation,'' Phys. Fluids **7**, 1184 (1995).

[33]H. C. Lee, ''Drop formation in a liquid jet,'' IBM J. Res. Dev. **18**, 364 (1974).
[34]D. B. Bogy, ''Drop formation in a circular liquid jet,'' Annu. Rev. Fluid Mech. **11**, 207 (1979).
[35]A. E. Green, ''On the non-linear behavior of fluid jets,'' Int. J. Eng. Sci. **14**, 49 (1976).
[36]S. E. Gechtel, C. D. Carlson, and M. G. Forest, ''Recovery of the Rayleigh capillary instability from slender 1-d inviscid and viscous models,'' Phys. Fluids **7**, 2956 (1995).
[37]R. M. S. M. Schulkes, ''The evolution and bifurcation of a pendant drop,'' J. Fluid Mech. **278**, 83 (1994).
[38]T. Y. Hou, J. S. Lowengrub, and M. J. Shelley, ''The long time motion of vortex sheets with surface tension,'' submitted to Phys. Fluids.
[39]L. Ting and J. B. Keller, ''Slender jets and thin sheets with surface tension,'' SIAM J. Appl. Math. **50**, 153 (1990).
[40]Y. J. Chen and P. H. Steen, ''Dynamics of inviscid capillary breakup: Collapse and pinchoff of a film bridge,'' to appear in J. Fluid Mech.
[41]W. van Saarloos, ''Front propagation into unstable states: Marginal stability as a dynamical mechanism for velocity selection,'' Phys. Rev. A **37**, 211 (1988).
[42]T. W. Shield, D. B. Bogy, and F. E. Talke, ''A numerical comparison of one dimensional fluid jet models applied to drop-on-demand printing,'' J. Comput. Phys. **67**, 327 (1986).
[43]J. B. Keller, A. King, and L. Ting, ''Blob formation,'' Phys. Fluids **7**, 226 (1995).